GA–A25640

THE GENERAL ATOMICS FUSION THEORY PROGRAM ANNUAL REPORT FOR GRANT YEAR 2006

by
PROJECT STAFF

OCTOBER 2006

GENERAL ATOMICS

DISCLAIMER

GA–A25640

THE GENERAL ATOMICS FUSION THEORY PROGRAM ANNUAL REPORT FOR GRANT YEAR 2006

by
PROJECT STAFF

Work supported by
the U.S. Department of Energy
under Grant No. DE-FG03-95ER54309

GENERAL ATOMICS PROJECT 03726
OCTOBER 2006

Abstract

The objective of the fusion theory program at General Atomics (GA) is to significantly advance our scientific understanding of the physics of fusion plasmas and to support the DIII–D and other tokamak experiments as well as ITER research activities. The program plan is aimed at contributing significantly to the Fusion Energy Science, the Tokamak Concept Improvement, and ITER goals of the Office of Fusion Energy Sciences (OFES).

1. Highlights of Theory Work in GY06

During the past year, considerable progress was made in each of the important areas of our research program:

- Significant progress was made in the development of the trapped gyro-Landau fluid (TGLF) transport model to replace GLF23. It includes development of a saturated turbulence amplitude model, tests against a GYRO transport database, and a fast linear-eigenmode code TGLF that yields accurate growth rates for drift-wave instabilities.

- Expensive gyrokinetic simulations of coupled ion temperature gradient/trapped electron mode-electron temperature gradient (ITG/TEM-ETG) turbulence using GYRO were carried out under INCITE06 with a number of striking conclusions: ITG/TEM and ETG transports are not strongly coupled, but coupled simulations are required for obtaining an accurate turbulence spectrum, and spectral isotropy eases high-k diagnostic measurements.

- Over 70 GYRO nonlinear simulations were carried out using Miller equilibrium model to extend the $E\times B$ shear quench rule to real geometry that will be incorporated in the TGLF transport model.

- Other GYRO simulations also yielded important results. These include large corrugations in T_e gradient when q_{min} = 2/1 passes into the plasma as seen experimentally, both ion and electron energy diffusivities decrease with plasma elongation due to less $E\times B$ shear needed to quench transport, and interaction of alpha particles with ITG modes is not negligible.

- A new theoretical model for edge localized mode (ELM)-free QH mode discharges was proposed and tested against experiments. The model postulates that QH mode exists in a low collisionality regime limited by a relatively low-n kink/peeling instability that is responsible for the edge harmonic oscillations.

- Three mechanisms were explored to explain the central current deficit in DIII-D hybrid discharges: magnetic curvature drift due to Alfvén wave (AW), kinetic AW mode conversion, and scattering of neutral beam injection (NBI) fast ions. Evaluations using DIII-D parameters indicate that particle drifts and mode conversion can effectively drive counter current.

- An analysis of DIII-D hybrid discharges just before onset of a 2/1 tearing mode finds that the tearing stability at q = 2 is highly sensitive to q(0) approaching unity, as a result of the rapid drop in the ideal β_N limit toward the experimental β_N.

- A fundamental formulation of the flux-surface-average energy continuity equation was developed from the six-dimensional collisional Vlasov equation with the neoclassical transport and heating separated from the turbulent transport and heating.

- A 64-bit parallel version of the global convergent Newton method solver GCNMP was developed that includes the basic tokamak transport equations with GLF23 as the primary energy transport vehicle.

- A detailed calculation for fast ion stabilization of the internal kink using the Porcelli model in two DIII-D L-mode discharges with giant and small sawteeth yielded results more consistent with the observed discharge behavior.

- A compact expression was obtained for the angular momentum flux in the Pfirsch-Schluter regime in the small rotation case in general geometry that predicts a negative slope of the toroidal flow near the edge as observed in many experiments.

- The enhanced shielding due to the $J \times B$ Lorenz force on the ionized ablation flow can significantly reduces the pellet ablation rate up to a factor of 2 to 3.

- A new similarity model to determine the conditions for spark ignition of a liner in magnetized target fusion was developed.

As a consequence of these results, scientists from the Theory Group were selected to give a number of invited talks and colloquia as highlighted in the next section. Following this are more detailed descriptions of the advances and achievements made in each of the major areas.

2. Significant Presentations in GY06

- P.B. Snyder gave two presentations "ELITE and Its Use in the Study of ELMs" and "Nonlinear 3D Simulations of ELMs with the BOUT code" at the ELM Modeling Workshop in Boulder, Colorado January 2006.

- J. Candy gave a seminar on "Coupled ITG/TEM-ETG simulations using GYRO" at the Department of Energy in Germantown, Maryland on February 15, 2006.

- J. Candy and P.B. Snyder gave two presentations "The GYRO Code: Turbulence in Tokamak Plasmas," and "Nonlinear Dynamics and Transport Mechanisms for ELMs: Physics of ELM-free QH and RMP Discharges" at the Transport Task Force (TTF) meeting in Myrtle Beach, South Carolina, April 4-7, 2006.

- P.B. Snyder gave a presentation "Physics of Steady-State ELM-free Quiescent H-Mode and RMP Regimes" at the pedestal ITPA meeting in Boston, Massachusetts, April 11, 2006.

- J.E. Kinsey gave an invited presentation "Parametric Dependencies of Transport Using Gyrokinetic Simulations Including Kinetic Electrons" at the combined 2006 APS and Sherwood meeting in Dallas, Texas, April 22-25, 2006.

- V.S. Chan, L.L. Lao, and R.E. Waltz made three invited presentations "Monte-Carlo Simulation of ICRF Wave Interactions with Energetic Particles in Tokamak Plasmas," "Tokamak and ITER Equilibrium Reconstruction," and "Continuum Gyrokinetic Simulations and Gyro-Fluid Models" at the ITER Simulation Workshop hosted by Peking University in Beijing, China, May 15-17, 2006.

- D.P. Brennan, M. Choi, P.B. Parks, and R.E. Waltz made four presentations "Resistive Stability of 2/1 Tearing Modes in DIII-D Plasmas with 1/1 Resonance," "Effects of Fast Ions Produced by Fast Wave Heating in Neutral Beam Injected Plasma on Sawteeth Activities in the DIII-D Tokamak," "A High-Velocity Microwave-Powered Pellet Launcher for ITER," and "Gyrokinetic Simulations of Off-axis Minimum-q Profile Corrugations" at the 33rd European Physical Society Meeting on Plasma Physics, in Rome, Italy, June 19-23, (2006).

- D.P. Brennan gave an invited presentation "Computing Nonlinear Magnetohydrodynamic Instabilities in Fusion Plasmas" at the SciDAC 2006 Conference in Denver, Colorado, June 25-29, 2006.

- A.D. Turnbull made a presentation "Monte-Carlo Simulation of High Harmonic Fast Wave Heating of Neutral Beam Ions and Effects on MHD Stability: Validation with Experiments" at the Workshop on Theory of Fusion Plasmas in Varenna, Italy, August 28 through September 1, 2006.

- J. Candy and J.E. Kinsey made two presentations "ETG Turbulence Coupled to ITG/TEM Turbulence" and "Database of Gyrokinetic Transport Simulations and Comparison to a New Comprehensive Theory-Based Transport Model" at the 11th EU-US Transport Task Force Workshop in Marseille, France, September 4-7, 2006.

- Four GA theory papers were selected for oral presentations at the 21st IAEA Fusion Energy Conference to be held in Chengdu, China, October 16-21, 2006, "Mechanism for Maintaining the Quasi-Steady State Central Current Density Profile in Hybrid Discharges" by M.S. Chu, "Stability and Dynamics of the Edge Pedestal in the Low Collisionality Regime: Physics Mechanism for Steady-State ELM-Free Operation" by P.B. Snyder, "A Comprehensive Theory-Based Transport Model" by G.M. Staebler, and "Coupled ITG/TEM-ETG Gyrokinetic Simulations" by J. Candy.

- Three GA theory papers were selected for invited presentations at the 48th APS DPP meeting to be held in Philadelphia, Pennsylvania, October 30th through November 3, 2006, "Resistive Stability of 2/1 Modes near 1/1 Resonance" by D.P. Brennan, "A Theory-Based Transport Model with Comprehensive Physics" by G.M. Staebler, and "Coupled ITG/TEM-ETG Gyrokinetic Simulations" by R.E. Waltz.

3. Advances in Transport Research

3.1. GYRO Development and Applications

The first year INCITE06 work on coupled ITG/TEM-ETG gyrokinetic simulations has been completed. All previous gyro-kinetic simulations of ETG assumed adiabatic ions. This has proven to be inadequate for cases at moderate shear. GYRO is the first gyro-kinetic code to treat ETG with kinetic ions. We performed very expensive high effective Reynolds number $R = (k_{max}/k_{min})^2$ GYRO simulations spanning the low-k ITG/TEM transport and the high-k ETG transport. These simulations required a large simulation box (at least $64\rho_{si} \times 64\rho_{si}$) to cover the large ion gyro-scale eddies while resolving the small electron gyro-scale eddies of the ETG. From $k_{min}\rho_{si} = 0.1$ to $k_{max}\rho_{se} = 0.7$, the number of toroidal modes is $k_{max}/k_{min} = 420(\mu/60)$ where $\mu = \rho_{si}/\rho_{se}$ is the ratio of ion to electron gyro-radii. The large simulation with $\mu = 30$ required 7-24 hour restarts on 768 processors (75%) of the X1E Cray Phoenix at NCCS-ORNL. A deuterium plasma has $\mu = 60$ but computational time scaling as $\mu^{3.5}$ precludes such simulations. Fortunately the simulations from $\mu = 20$ and $\mu = 30$ showed that, the $\mu = 30$ simulations were close to physical reality for the GA-standard case investigated.

The work yielded a number of striking conclusions. Defining low-k ITG/TEM transport to be that from $k_y\rho_{si} \le 1$ and high-k ETG transport to be that from $k_y\rho_{si} > 1$, we found that:

- The transport from ITG/TEM and ETG modes is not strongly coupled. The low-k ITG/TEM transport can be accurately simulated with large-box and low-resolution simulation as expected, and the high-k ETG electron energy transport can be accurately simulated with small-box and high-resolution simulations as long as the ETG drift waves can couple to some non-adiabatic ion zonal flows.

- However, to obtain a physically accurate spectrum of transport and $\delta n/n$ turbulence diagnostic, expensive coupled simulations are required.

- The spectra fall monotonically from a peak in the low-k ITG/TEM region, and the $\delta n/n$ turbulence diagnostic spectrum is remarkably isotropic at high-k. This significantly eases the high-k turbulence diagnostic measurements.

- It was found from artificially turning off the high-k drive that the $\delta n/n$ turbulence diagnostic is not very sensitive to the drive, and hence likely cannot detect the ETG instability.

- The ETG transport measured in ion gyroBohm units was found to be approximately invariant to μ. We looked at the GA-standard case with lower trapping which turns down the TEM drive and opens a stability gap between ITG and ETG ($0.9 < k_y\rho_{si} < 1.6$). Surprisingly, there was no gap in the transport spectrum. This is the first example of transport from nonlinear mode coupling and the first observed breakdown in the "per mode quasi-linear transport rule" used to build transport models like GLF23 (or the new TGLF). We also learned that fairly accurate spectra of transport and $\delta n/n$ turbulence diagnostics, as well as $E\times B$ shear stabilization can be obtained without going to extremely high resolution. For the GA-standard case, ETG transport was about 10% of the electron energy transport that in turn is about 30% of the total energy transport. As expected, we showed that the ETG mode survives the $E\times B$ shear quench of the low-k ITG/TEM transport and as expected, will dominate inside internal transport barriers.

An important consideration from ETG-ai simulations has been the existence of so called "streamers". Streamers are radially-elongated eddies to be expected when the zonal (y-directed) $E\times B$ flows are too weak to break up the radial (x-directed) $E\times B$ flows from the drift waves. It has long been argued that such streamers, while still on the electron gyro-radius scale, could still provide long radial correlation and account for the lack of isomorphy with ITG. However, when small electron-scale ETG eddies are embedded in the larger ion-scale eddies, streamers cannot be mathematically isolated by contour (level) plots (i.e. they cannot exist). As indicated in the large-scale $64\rho_{si} \times 64\rho_{si}$ contour plot shown in Fig. 1(a), any small electron-scale eddies can only appear as "fuzz" on the density contours of the ion eddies. However, as clear from the $8\rho_{si} \times 8\rho_{si}$ simulation shown in Fig. 1(b), 5:1 streamers do appear in the less-physical ETG $16\rho_{si} \times 8\rho_{si}$ small box simulations in which the periodicity does not allow the large-scale ions eddies to exist. The corresponding time-averaged density fluctuation $k_x - k_y$ spectrum for the large box coupled ITG/TEM-ETG and the small box uncoupled ETG-ki are shown in Figs. 1(c) and 1(d). It is clear that streamers, if they exit, have a less isotropic spectrum.

An extensive series of GYRO simulations, variants of a standard (STD) test case, was performed to create a gyrokinetic transport database. For simplicity, the simulations are electrostatic and consider only local effects. Variations of safety factor, magnetic shear $\hat{s}$, MHD α parameter, $E\times B$ shear, etc. have been treated. Both ITG and TEM-dominated regimes have been considered. The database of more than 300 nonlinear was used for benchmarking and to fit and test the new TGLF transport model.

Over 70 GYRO nonlinear simulations were also carried out using Miller equilibrium model to extend the $E\times B$ shear quench rule to real geometry that will be incorporated in the TGLF transport model. Two versions of the quench rule were derived to fit the

GYRO results. One version is to be used with the flux-surface-averaged *E×B* shear rate (as used in GLF23). The other version is to be used with the Hahm-Burrell *E×B* shear rate. The simulations consisted of a series of parameter scans varying elongation and aspect ratio over a range of $1 \le \kappa \le 2$ and $2 \le A \le 5$. Both versions fit the GYRO data well. In general, it was found that less *E×B* shear is needed to quench low-k ITG/TEM transport at high elongation and low aspect ratio.

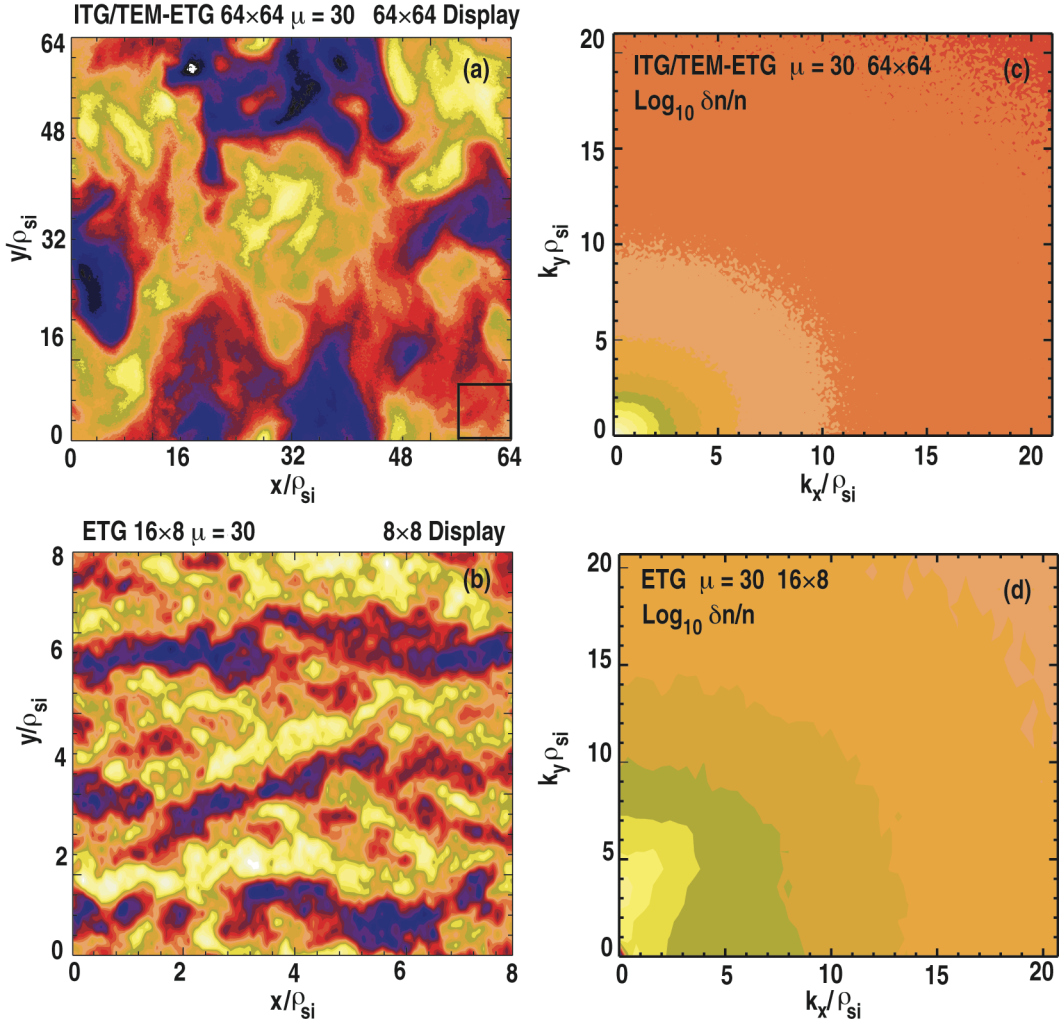

Fig. 1. x-y instantaneous density contour plots: (a) 64×64 ITG/TEM-ETG coupled simulation with 8×8 display guide box at lower left; (b) slice from 16×8 ETG uncoupled simulation displayed with 8×8 aspect ratio. Corresponding time average $k_x - k_y$ spectrum of density fluctuations: (c) 64×64 ITG/TEM-ETG coupled simulation; (d) 16×8 ETG uncoupled simulation.

Work to explore the effect of elongation (κ) on turbulent transport and *E×B* shear quenching using GYRO nonlinear simulations was continued. In simulations varying κ while holding all other quantities fixed, the normalized GYRO diffusivities robustly

exhibit an offset linear dependence. Power law fits yield a scaling of roughly $\kappa^{-1.0}$ for scans around the GA STD case using the Miller equilibrium model. These simulations were performed using non-periodic boundary conditions. To eliminate the possibility of boundary effects playing a role, a series of periodic boundary condition cases were performed and the same result was obtained (Fig. 2). Scans around the STD case with $a/L_T = 1.75$, which is close to the critical gradient, show a kappa scaling of $\kappa^{-1.3}$ which is somewhat stronger than the STD case result at $a/L_T = 3$. This suggests a zonal effect may be important near threshold. Simulations show that the GAM frequency decreases by 25% when κ is increased from 1.0 to 2.0.

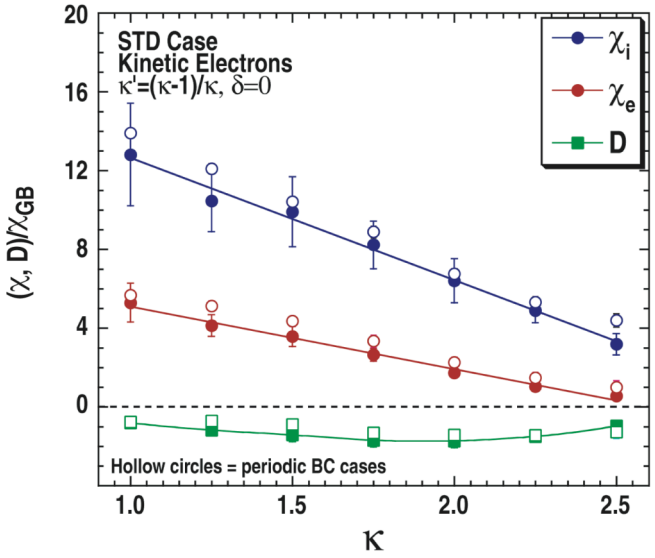

Fig. 2. Variation of time-averaged ion and electron energy diffusivities and particle diffusivity with elongation κ from GYRO nonlinear simulations with kinetic electrons around the STD case. The solid (hollow) points are with non-periodic (periodic) boundary conditions.

Nearly all work on turbulent confinement losses were focused on transport losses. Research by Hinton and Waltz on "Gyrokinetic Turbulent Heating" published in Physics of Plasmas provides a fundamental formulation of the flux surface average energy continuity equation starting from the six-dimensional collisional Vlasov equation. The neoclassical transport and heating are separated from the turbulent transport and heating. The latter are expressed as bilinear products of the gyrokinetic perturbed distribution function δf and self-consistent electromagnetic field $(\delta\varphi, \delta A_{||}, \delta B_{||})$ to be evaluated by GYRO simulations. An intermediate form of the energy continuity equation has the divergence of the plasma energy flux $\vec{\nabla}\cdot Q$ on the left hand side and on the right, turbulent heating $\delta\vec{j}\cdot\delta\vec{E}$ plus the heating from the electric fields $\vec{j}\cdot\vec{E}$. (The latter includes the work done by the radial turbulent transport flow against the radial electric fields.) For steady state turbulence, Poynting's theorem gives the turbulent heating as

$\delta\vec{j}\cdot\delta\vec{E} = -\vec{\nabla}\cdot\vec{F}$ where $\vec{F}$ is the Poynting flux carrying turbulent field energy. When the flux surface average $\vec{F}$ decreases with radius, the turbulence is heating the plasma and offsetting the radial transport losses in $\vec{\nabla}\cdot\vec{Q}$. The final form is written in terms of the standard gyrokinetic transport loss on the left $\vec{\nabla}\cdot\vec{Q}^G$ and a gyrokinetic heating H^G on the right. The paper treats the complete electromagnetic form, but in the electrostatic limit $H^G = -\vec{\nabla}\cdot\vec{Q}^\rho + \delta j_{||}\delta E_{||} + \vec{j}_{\perp d}\cdot\delta E_\perp$. $\vec{Q}^G = \delta\vec{\upsilon}_E\delta w$ is the usual $E\times B$ turbulent transport flux and $\vec{Q}^\rho$ is an additional and new finite gyro-radius turbulent transport flux. For the ions $\vec{Q}^\rho$ is about 10% of $\vec{Q}^G$. The term $\vec{j}_{\perp d}\cdot\delta E_\perp$ corresponds to a turbulent heating from the curvature and ∇B currents. Radially integrated, it offsets about $r/(2R)$ (i.e. at most 15%) of the gyrokinetic energy flux $\vec{Q}^G$. From preliminary GYRO evaluations $\delta j_{||}\delta E_{||}$ appears to offset another 10%-20% at most. Combining the turbulent heating and with the additional finite gyro-radius transport, we estimate a very modest 25% offset to the standard gyrokinetic transport flux. To put this in perspective, four of the five GYRO simulations of DIII-D discharges, have had power flows about two-fold in excess of the experimental flows (one produced two-fold underestimate). In the core, a two-fold excess can be compensated by a 10%-15% reduction in the ion temperature gradient (or 15% increase in $E\times B$ shear). Thus the offset is in the direction to improve agreement with experiment. Future GYRO simulations will account for the turbulent heating.

In collaboration with Klaus Hallatschek (IPP-Garching 2005 Rosenbluth Fellow), we are running full-physics GYRO edge simulations with DIII-D profile data. Shot 118897 has an L-edge phase and an H-pedestal. The simulations span $0.90 < r/a < 0.99$. This is a region of very high gradients, shears, and collisionality where we have little experience with running GYRO. We have found high-k_x and high-k_y numerical instability that we have partially under control. Finite β runs are difficult but possible at very small time steps. Nearly all the transport is packed at rather low k_y, at least much lower than typical of the code. Very preliminary results show the L-mode edge simulations in surprisingly close agreement with the experiment. Electrostatically, the H-pedestal phase has low transport in the range of the experimental levels, but finite β runs appear to exceed a critical β with enormously large transport. The motivation for the work is to try to delineate the parameters required for an L-H transport bifurcation, i.e. jump from low to high gradients at fixed transport power flow.

GYRO simulations of negative-central-shear DIII-D discharges show large corrugations in the T_e gradient as q_{min}= 2/1 passes into the plasma. The corrugations have the same bump-dip-bump structure as seen in the experiments. The corrugations are flux-surface and time averages of components of zonal flows, and as such constitute the first direct measurement of a zonal flow.

In a burning plasma, the alpha-particle population will be localized within the core ($r/a < 0.6$), whereas turbulence levels are generally weak for $r/a < 0.4$ and increase towards the edge. GYRO simulations in the vicinity of $r/a = 0.5$, where an overlap of alpha particles with ITG turbulence occurs, indicate that for ITER-like plasmas the turbulent alpha fluxes (both density and energy) can be as strong (per particle) as the turbulent D-T fluxes. This violates the common wisdom that the effects of turbulence on large-gyro-radius alphas are averaged out. This research ultimately indicates that in the outer band, $0.4 < r/a < 0.6$, alpha particle modeling codes may need to account for profile modification due to interaction with ITG turbulence.

Numerical 3D turbulence studies show a strong impact of magnetic geometry on the oscillating zonal flows known as geodesic acoustic modes (GAMs), a ubiquitous phenomenon detected five years ago that is prevalent near the tokamak edge. On one hand, changing the Shafranov shift, ellipticity, safety factor, or magnetic shear, individually alter the drive efficiency from Reynolds Stress, Stringer-Winsor force, and finite-Larmor-radius heat flux. On the other hand, geometric effects also couple the GAMs to various parallel sound waves, giving rise to complex interactions. A deep understanding of the experimental GAM amplitudes would open up a novel way to improve tokamak performance, since — at least in the simulations - dramatic reductions in transport are possible by choosing a GAM-optimized configuration.

3.2. TGLF Transport Model Development

Electromagnetic fluctuations were added to the TGLF equations. Both perpendicular and parallel magnetic field fluctuations were included. This requires several new Bessel function integrals to be included in the set of fitted numerical functions in the code. Work to find a quasi-linear mixing length rule for TGLF that yields the best fit to a GYRO database comprised of nonlinear simulations including kinetic electrons was also carried out. The database compilation was advanced to 86 cases. Various model have been tried. The models are in the form of a generalized mixing length rule that depends only on the linear growth rate, frequency and wave number of the most unstable mode. The particle and energy fluxes are computed by multiplying the saturation rule model by the quasi-linear weights found with the new TGLF eigenmode solver. The version that will be published in the 2006 IAEA proceedings has a 16% fractional deviation for the ion, 15% for the electron energy flux, and 28% for the particle flux for the whole data set. A new model for the "zonal flow shear" has been developed that fixes an unphysical feature of the growth rate cut-off used in previous versions. Running GLF23 for this database showed that TGLF is much more accurate, especially for the electron energy flux which is systematically too high for GLF23 (Fig. 3). Efforts will now focus on extending the fit and the GYRO database used in the model fitting to include real geometry.

The fast linear eigenmode code TGLF has been installed as an option in the gyro-kinetic stability analysis code GKS. TGLF is a new gyro-fluid system that yields accurate growth rates for drift-wave instabilities and includes nearly all of the same physics as GKS. The TGLF solver is fast enough to be able to perform between-discharge stability analyses in the DIII-D control room. A new feature of TGLF is the ability to compute growth rates for sub-dominant instabilities. The default settings for the GKS code include Miller shaped geometry, one impurity ion, electron-ion collisions and electromagnetic fluctuations. Analysis options for finding critical temperature gradient and maximum growth rate profiles and the mode spectrum at one location are all available for either the original GKS or the TGLF models.

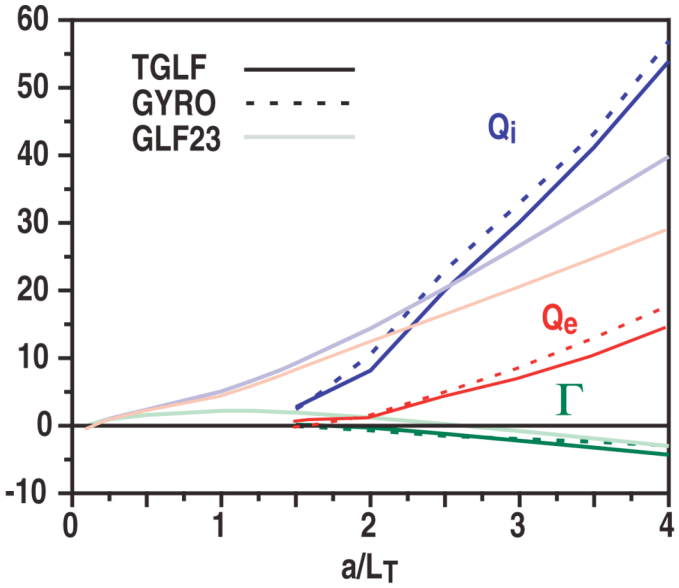

Fig. 3. Comparison of normalized fluxes for TGLF (solid), GYRO (dashed), and GLF23 (light solid) for a scan in a/L_{Ti}= a/L_{Te} about the GA-Standard point.

3.3. Transport Code and Module Development

A 64-bit parallel version of the Globally Convergent Newton Method (GCNM) solver was developed. The solver includes the basic tokamak transport equations as originally developed for the ONETWO code with GLF23 as the primary energy transport vehicle. The modular nature of GCNMP allows it to interact with all transport related physics codes (e.g. neutral beam, rf heating and current drive, MHD, etc.) In addition, GCNMP can utilize adaptive grids (variable size and spacing) and a variable number of equations by simply creating state files that include the necessary information. GCNMP is now being tested and will be installed shortly at PPPL and ORNL for use by the NTCC and SWIM projects.

A new version of the ONETWO transport code was developed that features full integration of the NUBEAM NTCC module, as well as the ability to run simpler and faster NFREYA-derived beam calculations for between-shot analysis in DIII-D. The NTCC Multi-mode confinement module MM95 was also added to ONETWO. A 64-bit version was also created that includes an interface to the new parallel GCNMP. The 64-bit version reduces the CPU time by about ~30%.

3.4. Transport Theory Development

Work on formulating a full-f conservative gyro-kinetic code was performed. The dynamical equation is conservative electro-statically or when change in the direction of the magnetic field can be neglected. Full-f conservative equations are needed when there is no clear separation between transport and turbulence scales as is the case near transport barrier formation. The formulation is most convenient in the magnetic moment and parallel velocity basis (μ, $v_{||}$). Unlike the GYRO δf code that used a locally normalized energy and pitch-angle basis, a full-f formulation cannot avoid velocity space gradients and (μ, $v_{||}$) is most convenient for collisions. The conservative drift kinetic equation recovers the [Hazeltine 1973] non-conservative form. The full-f gyrokinetic equation is obtained by replacing the field with their gyro-averages. A real space formulation in a field line following wedge is being studied. The intent is to understand how such a full-f system is to be implemented so as to recover GYRO δf flux-tube results at small ρ^*. This is a necessary step before such codes can be used for edge simulations.

A compact expression was obtained for the angular momentum flux in the Pfirsch-Schluter regime in the small rotation case in general geometry, under the additional assumption of low β and small poloidal field (in comparison with toroidal field). It reproduces an existing result for large-aspect-ratio circular cross-section flux surfaces. The same expression was obtained from both a fluid approach and a drift-kinetic approach, demonstrating the equivalence that was recently questioned. The expression predicts a negative slope of the co-current toroidal flow near the edge as observed in many experiments.

4. Advances in MHD Stability Research

4.1. Edge Stability and ELM Onset

A new theoretical model for ELM-free QH mode discharges was proposed, which postulates that QH mode exists in the low collisionality regime in which the edge bootstrap current is large, and the limiting instability is a relatively low-n kink/peeling mode rather than the usual intemediate-n peeling-ballooning modes responsible for ELMs. Strong flow shear in the QH mode edge stabilized high-n ballooning modes, but actually destabilizes low-n kink/peeling modes. These low-n kink/peeling modes, driven unstable both by current and rotation, are postulated to be responsible for the edge harmonic oscillation (EHO) observed during QH mode. The modes are able to saturate, rather than grow explosively like ELMs, due to their ability to dissipate their drive at relatively low mode amplitudes, via transport and coupling to the conducting wall. Transport driven by the saturated mode allows near steady state operation in QH mode. Extensive QH mode stability calculations support this model, notably including accurate predictions of the required density for QH mode operation in various shapes. The stability space for low triangularity and higher triangularity DIII-D discharges computed using ELITE is illustrated in Fig. 4. The postulated QH mode region (shaded) is accessible only at very low density in low triangularity discharges, but at higher triangularity is accessible at substantially higher density in agreement with observation.

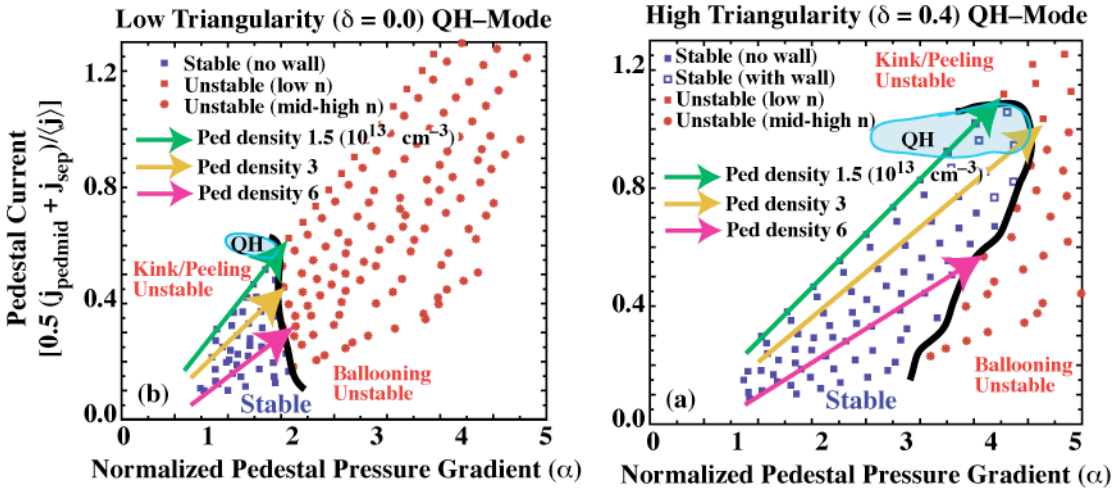

Fig. 4. Edge stability diagram for a low and a high triangularity discharge computed using ELITE showing the QH-mode parameter space.

A large set of 2006 RMP discharges in which ELMs are suppressed with an imposed RMP was also studied with ELITE. It is generally found that the RMP allows the discharge to maintain steady state pressure and current profiles below the peeling-ballooning stability boundary, allowing ELM-free operation.

Various improvements to ELITE were also made. By extending the expansion of rotation terms to higher order, we have found good quantitative agreement between the ELITE code and the MARS and CASTOR codes. The effect of sheared toroidal flows on growth rate, mode frequency and mode structure has been confirmed with all three codes. The inclusion and verification of toroidal flow shear in ELITE, now including higher order terms which scale as the product of the flow and the flow shear, allows accurate calculation of flow shear on MHD modes with mode numbers as low as n=5, while continuing ELITE's capability to efficiently calculate growth rates with flow shear for toroidal mode numbers as high as several hundred, much higher than previously existing codes. The physics of flow shear effects, stabilizing high-n modes while having a weak or even de-stabilizing effect on lower n modes has been confirmed.

In collaboration with N. Aiba from JAEA, ELITE has been successfully benchmarked with the MARG2D stability code. A number of TOQ-created equilibria have been studied, and good agreement has been found for both updown symmetric and asymmetric D-shaped equilibria and for a pure peeling mode test case.

4.2. Nonlinear ELM Study

We continued to study ELM physics using the resistive MHD code NIMROD on several series of model experimental equilibria prepared using discharges from the DIII-D ELM experiments. The equilibria being used as initial conditions have been distributed to CEMM for collaborating scientists to analyze and compare with our NIMROD results. All such results are contributing to the DOE Theory Milestone for 2006. In particular, kinetic equilibrium reconstructions based on DIII-D discharges 113207 and 113317 are being studied for linear stability and nonlinear evolution. Linearly unstable modes are in the range $5 < n < 25$ with the linear growth rates peaking at $n \sim 12$ for 113317 and $n \sim 15$ for 113207. Other modes are driven nonlinearly, some by two-wave interactions and some by three-wave interactions. The time evolution of the kinetic energy in toroidal modes 1-43 shows that the nonlinear mode structure is toroidally resolved with finger like structures near the plasma edge. Increasingly fine structures appear as the calculation progresses. The differences in the linear spectrum affect which modes are nonlinearly driven. The penetration depth of the nonlinear mode into the plasma from the edge is in reasonable agreement with experiment. Toroidal flow shears the structure of the nonlinear mode, reducing the amplitude of fluctuations

poloidally, and limits the extension of the filaments into the vacuum region, while having a smaller effect on the inward penetration.

The linear stability properties of a reconstructed DIII-D discharge equilibrium were also studied with the NIMROD code. The equilibrium is unstable to an edge-localized mode. The poloidal drift frequency ω_* for this case is peaked in the edge region where the electron pressure gradient is strongest. The stability analysis consequently included both the Hall and gyro-viscous effects. This was the first time these effects have been included in a calculation for ELMs in a real reconstructed DIII-D discharge. The Lundquist number S was approximately 2×10^7 and the Prandtl number was 0.1. The linear single-fluid growth rate spectrum with respect to toroidal mode number is peaked around n=10 and drops to marginality near n=20. In contrast, with the Hall and gyro-viscous terms included, the peak growth rate is reduced and mode numbers above n=16 are completely stabilized, but the low-n stability is weakly affected. This is in agreement with the conventional wisdom and with previous calculations for model equilibria. Future studies will include the Hall and gyro-viscous effects in the non-linear calculations.

4.3. 3/2 Mode Stability and q(0) in Hybrid Discharges

The role of the 3/2 mode in maintaining the quasi-steady state central current density profile in DIII-D hybrid discharges was investigated. Three mechanisms that provide the negative central current drive were studied. All rely on the development of a large co-rotating 2/2 sideband excited by the rotating 3/2 island. In the first mechanism, the central q(0) is assumed to develop to a value below the Alfvén resonance at the plasma center, yet above the value that initiates sawteeth. For the region within the Alfvén resonance, stationary kinetic Alfven Waves (KAW) are excited by the 2/2 sideband. The KAWs, due to their short perpendicular wavelengths, provide an efficient current drive counter to the plasma current within the resonant region. The mode conversion process is illustrated in Fig. 5. The amount of driven current increases quadratically with the size of the 2/2 side-band. In the second mechanism, the electric field sideband is excited by the 3/2 magnetic perturbations due to the magnetic curvature drift of the ions. This is a purely toroidal effect and contributes to the negative current drive over a larger range of q_0 values than the KAW mode conversion mechanism (Fig. 6). In the third mechanism, the magnetic perturbations due to the 3/2 and 2/2 modes are assumed to redistribute the energetic particle population from the NBI. This explanation is similar to a previous idea that proposes that toroidal Alfvén eigenmodes (TAEs) excited by the injected energetic beam ions due to low density result in a redistribution of the energetic particles. However, in the higher density hybrid discharges considered here, the TAEs are absent. We propose that scattering and redistribution of the energetic KAW particles is due to the 3/2 and 2/2 MHD perturbations. A set of magnetic perturbations was prepared and sent to Roscoe

White of PPPL to compute its effect on the energetic particles, including anomalous diffusion and expected current drive. Initial results indicate that the energetic particle density only modified modestly and this mechanism can account only for 10-20% of missing current.

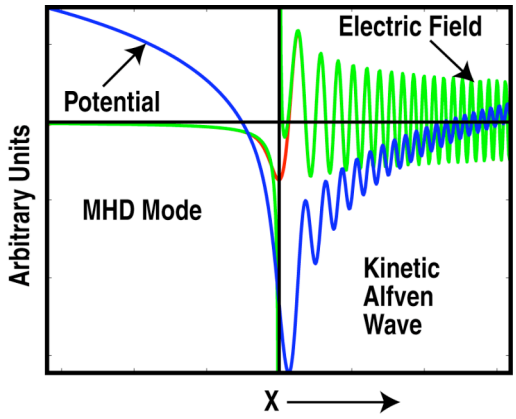

Fig. 5. Conversion of MHD perturbation (left) into KAW (right) at the mode conversion resonant surface at x = 0. Shown are electric potential (red) and electric field (blue) and analytic approximation by Airy functions (green).

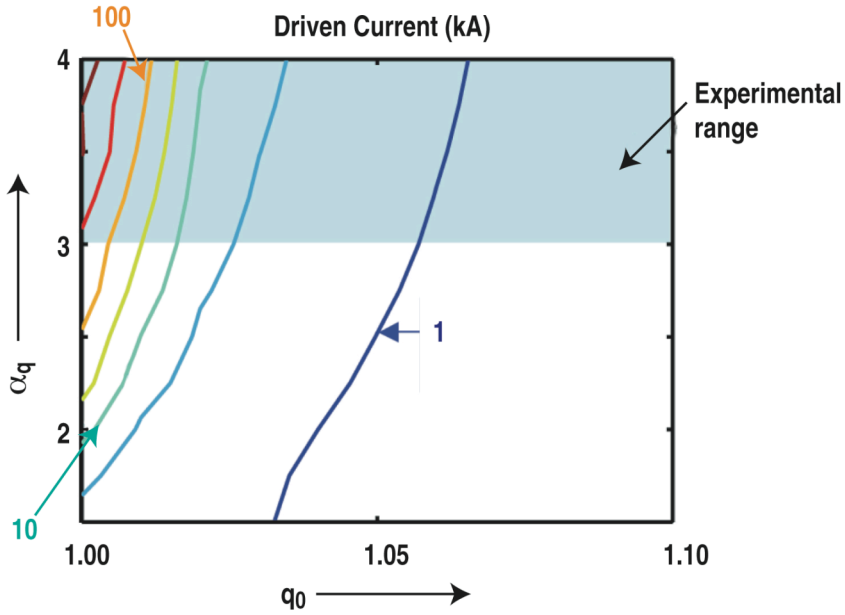

Fig. 6. Amount of negative central current drive in kA due to electric sidebands induced by magnetic curvature drift from Alfvén wave as a function of axial q(0) and q profile parameter α_q, $q = q_0 + (1.5 - q_0)(r / r_{3/2})^{\alpha q}$.

4.4. Low n Ideal Stability

Corrections to δW to restabilize the Alfvén continuum were implemented and shown to work extremely well in test cases. The Finite hybrid element method used in the GATO, ERATO, and KINX ideal MHD codes is well known to numerically destabilize the Alfvén continuum slightly. Localized continuum modes then converge from the unstable side to the marginal point quadratically with increasing mesh. The technique to restabilize these modes at a finite mesh, first used in the KINX code, was applied to the GATO representation. With the correction, numerically destabilized continuum modes were shifted to just slightly on the stable side ($\sim 10^{-7}$), leaving physically unstable modes hardly affected. Detailed convergence calculations confirm that the continuum is completely re-stabilized in each case for all mesh sizes.

Calculations using this new GATO version for the ideal internal kink mode in both DIII-D discharge and model circular cross section equilibria with q below one and slightly inverted shear revealed a sequence of unstable n = 1 ideal modes that are global eigenmode manifestations of Mercier instability. They occur in only certain special situations. These modes exhibit the Sturmian behavior expected from spectral theory for the ideal MHD operator that the eigenvalues are ordered strictly with the number of zero crossings. Numerically, the eigenvalues extend into the stable continuum and full convergence studies are needed to confirm if they actually have an accumulation point at marginal stability. This has implications for the plasma response to external perturbations since with no wall the modes also perturb the boundary and therefore contribute to the plasma response to an external perturbations.

Code modifications for a stability index analysis were implemented in GATO as the continuum is numerically re-stabilized and the numerical marginal condition coincides with the true marginal condition. It is simple now to run the GATO code to check only if the equilibrium is stable or not. This takes less than 30 seconds for up-down symmetric cases with a moderate mesh of $N_\psi \times N_\chi = 100 \times 200$.

In collaboration with Sherry Li of LBNL, the eigenvalues produced by the SuperLU fast parallel eigenvalue solver were shown to agree with those from GATO to three figures for a small grid representative test case. Initial results confirmed a factor 2 to 3 speedup. A series of larger grid cases are being set up to test the scaling of the speedup with mesh size. The speedup will allow GATO to be used to compute the full mode spectrum as a basis for describing the plasma response to external perturbations.

4.5. Resistive Stability

The MHD and two-fluid growth rates of a low β m=2/n=1 tearing mode in the presence of well-separated central sawtooth oscillations were examined using reconstructions of experimental DIII-D equilibria. The outer ideal MHD solutions between the rational q=1, 2, and 3 surfaces were determined using the PEST3 code for a low β equilibrium and the outer region solution was matched asymptotically to the Glasser, Greene and Johnson resistive MHD inner layer solutions. This yields a dispersion relation for the linear growth rate in the form of a matrix equation for the matching conditions. The most important effects in the dispersion relation are found to be the resistive interchange parameter D_R and the coupling to the 1/1 surface, both of which were stabilizing in the case considered. Two-fluid diamagnetic effects reduce the growth rates significantly, while inducing a mode rotation near the electron diamagnetic frequency. It is expected that this will be important for large diamagnetic frequencies since the rotation shear between surfaces will then significantly affect the coupling between them through the ideal matching data.

In many DIII-D hybrid discharges, the high performance phase is terminated by the growth of a large 2/1 tearing mode. Analysis of DIII-D hybrid discharges just before onset of a 2/1 tearing mode finds that the tearing stability at q = 2 is highly sensitive to q(0) (q_{min}) approaching unity, as a result of the ideal β_N limit rapidly decreasing toward the experimental β_N (Fig. 7). The analysis is based on experimental equilibria with q(0) constrained within the uncertainty of the reconstruction between 0.98 and 1.05. Varying q(0) in this range results in little or no change in the equilibrium near q=2 or elsewhere. For $q(0) \geq 1.02$, the 2/1 tearing stability is only weakly dependent on β_N. However, when $q(0) \leq 1.01$, the 2/1 tearing mode (at q = 2) becomes strongly unstable as the equilibrium approaches the n=1 ideal limit. This suggests that the proximity to the q=1 resonance is critical to the 2/1 tearing mode stability, and is responsible for the onset of the mode. The results suggest that the 2/1 onset may be prevented by a slight increase in q(0). The role of coupling to the 1/1 and 3/1 surfaces is currently being investigated using NIMROD.

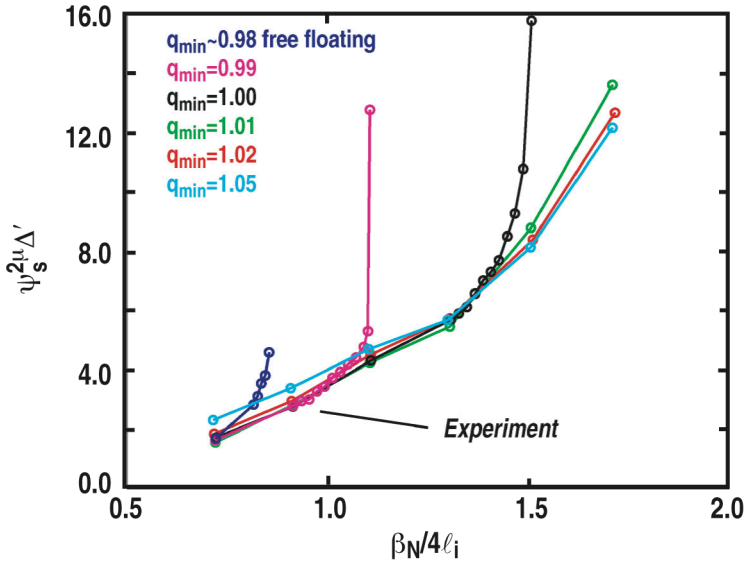

Fig. 7. The linear stability indexes for several series of equilibria with decreasing q_{min} by constraint on axis, and increasing pressure while holding q fixed. The ideal beta limit drops drastically as q_{min} approaches 1, causing the 2/1 tearing mode to go linearly unstable.

4.6. Non-Sxisymmetric Plasma Response

Several key results were obtained in the theoretical formalism of the plasma response to external non-axisymmetric perturbations. For the linearized response, the conditions for completeness of the 2D eigenfunctions of the ideal MHD operator, as a basis for the plasma response, were obtained. Completeness can be lost following projection on the plasma boundary and then inversion back to the full plasma domain. In addition to the obvious case where internal modes exist, the conditions can be violated in certain well-defined situations that can be easily monitored and possibly avoided. In addition, the Nuhrenberg-Boozer application for determining the resonant displacement jumps and associated island sizes was generalized to any (including non-resonant) response feature. The generalization can then be applied to determine the specific externally applied perturbations needed to induce non-resonant perturbations, for independent control of MHD modes and plasma rotation. GATO continuum modifications described in a previous section will enable GATO to be utilized as a numerical tool to implement this formulation.

5. Advances in RF Heating and Fueling Research

5.1. Interactions of ICRF Wave With Ions

Resonant interaction between ions and ICRF wave at arbitrary cyclotron harmonics has been usually treated as a diffusive process in velocity space. This assumes de-correlation in the relative phase difference of the wave and ions between successive resonances. In a collisionless high temperature plasma, the change in trajectory of ions due to the change of energy through this interaction may produce a de-correlated phase. Since the de-correlation of phase difference depends strongly on the combination of applied amplitude of ICRF wave, the wave frequency, and the energy of ions, stochastic threshold amplitudes of the wave above which non-adiabatic interaction takes place may be very different in fundamental thermal minority ion heating (C-Mod) and high harmonic energetic beam ion heating (DIII-D) cases.

ORBIT-RF was applied to study the stochastic behavior of ion orbits and evaluate the stochastic threshold in the wave electric field amplitude using 2-D mapping in phase space on the C-Mod and DIII-D tokamaks. For the fundamental harmonic C-Mod case, circulating thermal ions exhibit stochastic behavior in phase space at $E_+ = 1$ kV/m while trapped thermal ions interact with the wave efficiently even at $E_+ = 0.1$ kV/m, leading to more rapid randomization in phase space. In a scenario using 80 keV beam ion heating at 8th harmonic in DIII-D, a much larger electric field is required for efficient heating of the trapped energetic beam ions (>10 kV/m). However, circulating energetic ions appear to be still super-adiabatic even at high $E_+ = 10$ kV/m. More quantitative benchmarking with both analytical and numerical solutions from the full wave ICRF solver is underway.

5.2. Interactions of ICRF Fast Ions With Sawteeth

Stability calculations in support of the fast-ion stabilization studies of DIII-D discharges with the Porcelli model showed that there are some significant differences from the predictions of the analytic, large aspect ratio, circular cross section Bussac model for the ideal internal kink, depending on a specific equilibrium. For reconstructed equilibria in discharges with large sawteeth, the eigenfunction has approximately the "Top-Hat" structure of the Bussac model where the Porcelli model is applicable. For a discharge with much smaller sawteeth, however, the eigenfunction shape is significantly different from the assumed model. GATO calculations show that the difference in structure of the eigenfunctions is due to the change in the position of the $q = 1$ surface, $r(q=1)$, rather than to a change in the safety factor q on axis. As $r(q = 1)$ increases the

computed eigenmode becomes closer to "Top Hat" model. In addition, both the growth rate and marginal point can be sensitive to removing the wall with little visible change in the mode structure. This, the so-called "toroidal kink" mode, has been noted in previous studies of model equilibria. For real discharges, the Porcelli model incorporating the Bussac internal kink will need to be extended to account for these deviations.

A new refined calculation for fast ion stabilization of the internal kink using the Porcelli model in the same two DIII-D L-mode discharges with giant and small sawteeth yielded results more consistent with the observed discharge behavior. The refinement used a new more realistic formula for the ideal contribution to δW obtained by the Lausanne group from fitting numerically calculated growth rates to equilibrium shape parameters. In the earlier analysis, the fast ion contribution was sufficient to stabilize the ideal internal kink for the discharge with giant sawteeth. For the discharge exhibiting small sawteeth, however, the analytic Bussac model for the internal kink used in that analysis predicted stability even before the rf is on. With the new analysis, both discharges are predicted to be ideally unstable, consistent with both the ideal numerical stability calculations from GATO and the observed sawtoothing behavior of the discharges.

5.3. Pellet Ablation

A new 2D magneto-hydrodynamic simulation of pellet ablation in the electrostatic approximation was developed in collaboration with R. Samulyak and T. Lu of BNL. The major conclusion of the study is that in purely hydrodynamic simulations (without the J×B force), changing the heat flux deposition from spherically symmetric 1D to axisymmetric 2D leads to a minor reduction in the ablation rate, contrary to the prevailing expectation of a "factor of 2" reduction. However, in the magnetohydrodynamic simulations with the J×B force included, the magnetic field channels the flow into an extended plasma shield and significantly reduces the ablation rate by a factor of 2 to 3, depending on the time it takes for the heat flux to ramp up as seen by a moving pellet. Fast pellets crossing pedestal regions in ITER would lead to shorter warm-up times, which in turn lead to narrower ablation channels, stronger shielding, and reduced ablation rates.

5.4. Disruption Mitigation Using Massive Gas Injection

Modeling of the ORNL Mark IV massive gas injector (MGI) configuration for disruption mitigation using the 2D compressible fluid dynamic code FLUENT predicts rise times of 11 ms to reach the exit pressure and flow flattop from the time of the valve trigger for DIII-D, in agreement with measured exit pressure rise data. Calculations for

long times > 10 ms agree with test stand measurements of the "apparent steady" exit flow rate of 3.28×10^{24}/s for argon gas. All exit flow variables have a finite "rise time" resulting from a transient period while the gas flow adjusts asymptotically to its "apparent steady" rate. We can now confidently predict how many particles are injected during the first 8 ms period over which thermal quench begins and ends. In a typical discharge, e.g. #122516, the "mixing efficiency" is 9.2%, which is the fraction of injected particles assimilated by the plasma due to large-scale MHD mixing processes. By providing meaningful interpretations of MGI experiments on DIII-D, these calculations are contributing to understanding of the unsteady gas flow in the jet delivery tube that is required in order to make projections for disruption mitigation on ITER.

6. Advances in Innovative Confinement Concept Research

6.1. 3-D Equilibrium Reconstruction

Work to develop a 3D filament code MFIT3D for reconstruction of magnetic topology in stellarators and tokamaks with error or externally imposed toroidally asymmetric magnetic field was continued. The plasma current distribution is modeled using toroidally asymmetric current filaments. MFIT3D is computationally inexpensive and capable of handling magnetic islands and stochasticity. This development is complementary to the ongoing collaboration with ORNL and Auburn University to build the V3FIT 3D reconstruction code that is based on VMEC and assumes nested flux surfaces.

6.2. Magnetic Target Fusion (MTF)

In plasma jet Magnetized Target Fusion (MTF), a spherical array of discrete plasma jets are launched from the wall of a target chamber and form an imploding plasma liner. In one embodiment of this concept (D. Ryutov, FST 2006), the liner (inner layer of which is gold), is deeply subsonic, and cannot achieve a fusion energy gain G greater than unity (MTF needs $G \geq 10$ to be considered a practical energy source).

In our approach, we use supersonic DT jets, which merge at a smaller radius to make a thin imploding "shell liner". The advantage is to obtain high gain thermonuclear implosions $G \sim 10$ by burning a portion of the imploded DT liner. In an earlier study of this concept (2003-2005) we found that even under the most optimistic conditions — no oblique shocks formed when jets first begin to merge — very high Mach number $M \sim 60$ jets were needed to achieve high stagnation (hammer) pressures ~100 Mbar: implosion conditions necessary in MTF to ignite the central magnetized plasma target and form a thermonuclear "hot spot". During this year we found one improvement that enabled us to use lower Mach number jets. We considered jets that are very weakly ionized to begin with. Then by taking into account the *ionization energy sink* occurring during compressional heating of the imploding plasma liner, the liner temperature is "clamped", allowing for a high hammer pressure on target.

To achieve high fusion energy gain, we must rely on igniting and burning a portion of the cold dense fuel or liner by heat deposition from alpha particles released from the ignited hot-spot. We also developed a new 'similarity' model to determine the conditions

for liner ignition. The key ingredient in the model is that the stopping length of the alpha particles incident on the inner liner layer increases with liner temperature. The model indicates that magnetized target hot spots, which achieve ignition at *much lower* burn fraction than ICF targets, may not produce liner temperatures high enough to "fire-up" the liner fuel. Ignition of liners is therefore not straightforward, and may require new physics such as range shortening effects due to the magnetic field penetration ~ a magnetic skin depth into the liner surface. This idea will be investigated next year.

7. Publications and Activity

7.1. Publications with Primary Theory Authors

1. Brennan, D.P., and L.E. Sugiyama "Tearing Mode Stability in a Low Beta Plasma with Sawteeth," Phys. Plasmas **13,** 052515 (2006).

2. Brennan, D.P., *et al.,* "Computing Nonlinear Magnetohydrodynamic Edge Localized Instabilities in Fusion Plasmas," J. Phys.: Conf. Ser. **46,** 63 (2006).

3. Candy, J., and R.E. Waltz "Velocity–Space Resolution, Entropy Production, and Upwind Dissipation in Eulerian Gyro-Kinetic Simulations," Phys. Plasmas **13,** 03231 (2006).

4. Candy, J., R.E. Waltz, S.E. Parker, and Y. Chen "Relevance of the Parallel Nonlinearity in Gyrokinetic Simulations of Tokamak Plasmas," Phys. Plasmas **13,** 074501 (2006).

5. Choi, M., V.S. Chan, R.I. Pinsker, *et al.,* "Simulation of Fast Alfvén Wave Interaction with Beam ions over a Range of Cyclotron Harmonics in DIII-D Tokamak," Nucl. Fusion **46,** S409 (2006).

6. Chu, M.S, V.S. Chan, P.A. Politzer, *et al.,* "Kinetic Alfvén Wave and Associated Current Drive at Center of Tokamaks," to appear in Phys. Plasmas.

7. Estrada-Mila, C., J. Candy, and R.E. Waltz "Density Peaking and Turbulent Pinch in DIII-D Discharges," Phys. Plasmas **13,** 074505 (2006).

8. Estrada-Mila, C., J. Candy, and R.E. Waltz "Turbulent Transport of Alpha Particles and Helium Ash in Reactor Plasmas," to appear in Phys. Plasmas.

9. Hinton, F.L., and R.E. Waltz, "Gyrokinetic Turbulent Heating," Phys. Plasmas **13,** 102301 (2006).

10. Kinsey, J.E., R.E. Waltz, J. Candy "The Effects of Safety Factor and Magnetic Shear on Turbulent Transport in Nonlinear Gyrokinetic Simulations," Phys. Plasmas **13,** 022305 (2006).

11. Parks, P.B. "A Model of Cusp Magnetic-Field Compression by an Expanding Plasma Fireball," Phys. Plasmas **12,** 102510 (2005).

12. Parks, P.B., and F.W. Perkins "A Gyrotron-Powered Pellet Accelerator for Tokamak Refueling," Nucl. Fusion **46,** 770 (2006).

13. Snyder, P.B., H.R. Wilson, and X.Q. Xu, "Nonlinear Dynamics of ELMs: Numerical Studies of Flow Shear Effects and 3D Nonlinear ELM Dynamics," Phys. Plasmas **12**, 056115 (2005).

14. Staebler, G.M., J.E. Kinsey, R.E. Waltz "Gyro-Landau Fluid Equations for Trapped and Passing Particles," Phys. Plasmas **12,** 102508 (2005).

15. Staebler, G.M., and H.E. St. John "Predicted Toroidal Rotation Enhancement of Fusion Power Production in ITER," Nucl. Fusion **46,** L6 (2006).

16. Waltz, R.E., M.E. Austin, K.H. Burrell, and J. Candy, "Gyrokinetic Simulations of Off-Axis Minimum-q Profile Corrugations," Phys. Plasmas **13,** 052301 (2006).

17. Waltz, R.E., J. Candy, and C.C. Petty "Projected Profile Similarity in Bohm and GyroBohm Scaled DIII-D L- and H-Modes," Phys. Plasmas **13,** 072304 (2006).

7.2. Activity

- Dr. Klaus Hallatschek completed his one-year visit to the GA Theory Division as the 2005 Rosenbluth Award Recipient and returned to the Max-Planck Institute of Plasma Physics in Garching, Germany.

- Dr. Chris Holland joined the GA Theory Division for a one-year visit as the 2006 Rosenbluth Award recipient. Dr. Holland received his doctoral degree from the physics department of the University of California, San Diego. He is currently an assistant research scientist in the Center for Energy Research at UCSD.

- Emily Belli arrived at GA to work as an ORISE Postdoctoral Fellow on developing gyrokinetic-based computational models for studying tokamak edge plasmas.

- Carlos Estrada-Mila successfully defended his doctoral thesis at UCSD "Gyrokinetic Studies of Particle Transport in Tokamaks." Carlos was supervised by J. Candy and R.E. Waltz.

- The Second post APS Error Magnetic Field Workshop organized by Lang Lao was successfully held at the Adam's Mark Hotel in Denver, Colorado on October 28, 2005 with more than 40 participants**.**

- A GYRO development workshop was held at GA during the week of January 16-20, 2006. Users from PPPL, ORNL and the University of Texas came to contribute to the development of new standards for experimental profile data, and to refine the TRANSP-GYRO and ONETWO-GYRO interfaces. In addition, two days of the meeting were devoted to more general-interest GYRO lectures, which were attended by three graduate students from UCLA as well as more seasoned GYRO users. The final deliverable is the release of a much improved, polished and documented version 5.0.0 of GYRO.

- Dr. S. Guo from the RFP Group in Frascati visited GA for 4 weeks to collaborate with Ming Chu on the physics aspects of resistive wall modes common to RFPs and tokamaks and on related MHD phenomena.

- Dr. D.P. Brennan completed his assignment at GA first as an ORISE Postdoctoral Fellow and then as a visiting MIT research scientist and joined University of Tulsa as a professor in the Department of Physics and Engineering Physics.